Insight into the ATRP Rate Controlling Ability of Initiator Structure: Micromolecular, Macromolecular, and Immobilized Initiators

Yin-Ning Zhou, Zheng-Hong Luo

Department of Chemical Engineering, School of Chemistry and Chemical Engineering, Shanghai Jiao Tong University, Shanghai 200240, People's Republic of China
Correspondence to: Professor Z.H. Luo (E-mail: Luozh@sjtu.edu.cn)

Received 24 February 2014; accepted 10 May 2014; published online 2 June 2014
DOI: 10.1002/pola.27249

ABSTRACT: The equilibrium constant (K_{ATRP}) is a key factor for ensuring a successful atom transfer radical polymerization (ATRP), which guarantees a controlled process with predictable product properties. In this work, the effect of initiator type (i.e., micromolecular, macromolecular, and immobilized initiator) on the ATRP kinetics was studied through a developed mathematical model. It was validated thoroughly via experiments using fluorinated monomer (2,2,3,3,4,4,4-heptafluorobutyl methacrylate) as model component. The results show that the activity and deactivity of the copper(I) chlorine/1,1,4,7,7-pentamethyldiethylenetriamine ($Cu^{I}Cl$/PMDETA) heterogeneous catalytic complex is the highest for ethyl 2-bromoisobutyrate (Eib-Br), lower for bromo-poly(styrene) (PS-Br), and the lowest for bromo-aminopropyl functionalized SiO_2 (SiO_2-APTS-Br). The initiation system of Eib-Br with $Cu^{I}Cl$/4,4′-dinonyl-2,2′-bipyridyl (dNbpy) has relatively lower activating ability, but the polymerization keeps controllable by its higher deactivating ability. In addition, this homogeneous catalytic system ($Cu^{I}Cl$/dNbpy) is facile for further implementing the developed model to guide for the preparation of fluorinated gradient copolymers by semi-batch ATRP. © 2014 Wiley Periodicals, Inc. J. Polym. Sci., Part A: Polym. Chem. **2014**, *52*, 2228–2238

KEYWORDS: atom transfer radical polymerization (ATRP); initiators; kinetic modeling; method of moments; SI-ATRP; simulations

INTRODUCTION In recent years, quasiliving polymerizations are recognized to be the convenient techniques for preparing polymers with well-defined chain structures, for example, anionic, cationic polymerization, and reversible-deactivation radical polymerization (RDRP) techniques.[1–3] Atom transfer radical polymerization (ATRP) is known as a robust RDRP method in well controlling the molecular weight, polydispersity, and high retention of chain-end functionality, as well as facilitating high grafting density on solid surface.[4–6] Fluorinated polymers attract much interest due to a wide range of applications, such as thermoplastics, elastomers, and materials with low surface energy.[6–8] Recently, Luo et al.[9–13] reported a series of fluorinated copolymers with excellent properties via ATRP, such as poly(dimethylsiloxane)-*b*- poly(2,2,3,3,4,4,4-heptafluorobutyl methacrylate) (PDMS-*b*-PHFBMA),[9,10] poly(styrene)-*b*-PHFBMA,[11] and poly[2,7-(9,9-dihexyl fluorine)]-*b*-PHFBMA diblock copolymers,[12] as well as poly(acrylic acid-*grad*-HFBMA) gradient copolymers.[13] Besides, polymer/nanoparticle composite materials synthesized by surface-initiated ATRP (SI-ATRP) have also received much attention due to the combination of both the properties of the inorganic nanoparticles and those of the polymers.[14–20]

Many research works focus on the kinetic modeling for ATRP besides experiment study, while still few open reports are on the numerical investigation of the effect of initiator type on quasiliving ATRP kinetics.[21–45] Zhu and coworkers[21–25] first developed a kinetic model and investigated the effect of diffusion limitation on ATRP, and then extended into control over copolymer composition distribution in the semi-batch ATRP. Tobita[26–28] discussed the modeling of quasiliving radical polymerization kinetics in miniemulsion system. Recently, our group demonstrated the relationship among synthesis methodology, molecular structure and materials properties through theory and mathematic models.[29–31] Reyniers et al. and Soares et al. not only used the method of moments and Monte Carlo simulation, but also applied commercial software-PREDICI to study the kinetics of ATRP.[32–38] Simulation and theoretical studies for SI-ATRP have also been carried out, although they are all about the process of initiation from planar substrates.[39–45] More recently, Zhu and coworkers[41,42] proposed a new termination mechanism of SI-ATRP, providing mechanistic insight into the surface polymerization. In addition, Genzer and coworkers[43–45] used Monte Carlo simulation to compare

Additional Supporting Information may be found in the online version of this article.

TABLE 1 Elementary Reactions of ATRP

Type of reaction	Scheme
Initiation	$P_0X + C \xleftrightarrow{K_{eq}} P_0\cdot + CX$
	$P_0\cdot + M_i \xrightarrow{k_{in,i}} P_{1,i}\cdot$
Propagation	$P_{r,i}\cdot + M_j \xrightarrow{k_{p,ij}} P_{r+1,j}\cdot$
ATRP Equilibrium	$P_{r,i}X + C \xleftrightarrow{K_{eq}=k_a/k_{da}} P_{r,i}\cdot + CX$
Transfer	$P_{r,i}\cdot + M_j \xrightarrow{k_{tr,ij}} P_r + M\cdot$
Termination	$P_{r,i}\cdot + P_{s,j}\cdot \xrightarrow{k_{td,ij}} P_r + P_s$
	$P_{r,i}\cdot + P_{s,j}\cdot \xrightarrow{k_{tc,ij}} P_{r+s}$

the difference between ATRP initiated in bulk and on flat substrates.

As previously investigated through both theoretical and experimental approaches, polymerization kinetic parameters not only depend on temperature, pressure, and halogen (X), but also are influenced by ligand and initiator structure.[45–56] Our present work focuses on the numerical investigation for estimating various ATRP equilibrium constants using different initiator types and catalytic complexes. The simulations are carried out based on a comprehensive mathematical model and the method of moments, which are validated by experimental study using fluorinated monomer, micromolecular/macromolecular/immobilized initiator and heterogeneous catalytic complexes (CuCl/PDMETA). It should be noted that the immobilized initiator studied in this work is spherical nanoparticles. Furthermore, the presented model will be further implemented to guide the preparation for fluorinated gradient copolymers using an initiation system of ethyl 2-bromoisobutyrate (Eib-Br) with $Cu^{I}Cl$/dNbpy homogeneous catalytic complexes, which is appropriate for semi-batch ATRP.

MODEL DEVELOPMENT

Batch and Semi-Batch ATRP Kinetic Equations

The elementary reactions of ATRP or ATRcoP are listed in Table 1 on the basis of some confirmed assumptions.[24,29,35]

TABLE 2 Kinetic Equations for Type of Chain Species

Type of Chains	Mass Balance Equations
Solution Homopolymerization	
Propagating Radical	$\frac{d[P_{r,i}\cdot]_{sol}}{dt} = k_p[P_{r-1,i}\cdot]_{sol}[M_i]_{sol} - k_p[P_{r,i}\cdot]_{sol}[M_i]_{sol} + k_a[P_{r,i}X]_{sol}[C]_{sol}$ $- k_{da}[P_{r,i}\cdot]_{sol}[CX]_{sol} - k_{tr}[P_{r,i}\cdot]_{sol}[M_i]_{sol} - (k_{tc}+k_{td})[P_{r,i}\cdot]_{sol}\sum_{s=1}^{\infty}[P_{s,i}\cdot]_{sol}$
Dormant	$\frac{d[P_{r,i}X]_{sol}}{dt} = k_{da,i}[P_{r,i}\cdot]_{sol}[CX]_{sol} - k_{a,i}[P_{r,i}X]_{sol}[C]_{sol}$
Dead	$\frac{d[P_r]_{sol}}{dt} = k_{tr}[P_{r,i}\cdot]_{sol}[M_i]_{sol} + k_{td}[P_{r,i}\cdot]_{sol}\sum_{r=0}^{\infty}[P_{r,i}\cdot]_{sol} + \frac{k_{tc}}{2}\sum_{s=0}^{r}[P_{r,i}\cdot]_{sol}[P_{r-s,i}\cdot]_{sol}$
Surface Homopolymerization	
Propagating Radical	$\frac{d[P_{r,i}\cdot]_{surf}}{dt} = k_p[P_{r-1,i}\cdot]_{surf}[M_i]_{sol} - k_p[P_{r,i}\cdot]_{surf}[M_i]_{sol} + k_a[P_{r,i}X]_{surf}[C]_{sol}$ $- k_{da}[P_{r,i}\cdot]_{surf}[CX]_{sol} - k_{tr}[P_{r,i}\cdot]_{surf}[M_i]_{sol} - (k_{tc}^{surf}+k_{td}^{surf})[P_{r,i}\cdot]_{surf}\sum_{s=1}^{\infty}[P_{s,i}\cdot]_{surf}$
Dormant	$\frac{d[P_{r,i}X]_{surf}}{dt} = k_{da,i}[P_{r,i}\cdot]_{surf}[CX]_{sol} - k_{a,i}[P_{r,i}X]_{surf}[C]_{sol}$
Dead	$\frac{d[P_r]_{surf}}{dt} = k_{tr}[P_{r,i}\cdot]_{surf}[M_i]_{sol} + k_{td}^{surf}[P_{r,i}\cdot]_{surf}\sum_{r=0}^{\infty}[P_{r,i}\cdot]_{surf}$ $+ \frac{k_{tc}^{surf}}{2}\sum_{s=0}^{r}[P_{r,i}\cdot]_{surf}[P_{r-s,i}\cdot]_{surf}$
Solution Copolymerization	
Propagating Radical	$\frac{d[P_{r,i}\cdot]_{sol}}{dt} = \sum_j k_{p,ji}[P_{r-1,j}\cdot]_{sol}[M_i]_{sol} - \sum_j k_{p,ij}[P_{r,i}\cdot]_{sol}[M_j]_{sol} + k_{a,i}[P_{r,i}X]_{sol}[C]_{sol}$ $- k_{da,i}[P_{r,i}\cdot]_{sol}[CX]_{sol} - \sum_j k_{tr,ij}[P_{r,i}\cdot]_{sol}[M_j]_{sol} - \sum_j\sum_s (k_{tc,ij}+k_{td,ij})[P_{r,i}\cdot]_{sol}[P_{s,j}\cdot]_{sol}$
Dormant	$\frac{d[P_{r,i}X]_{sol}}{dt} = k_{da,i}[P_{r,i}\cdot]_{sol}[CX]_{sol} - k_{a,i}[P_{r,i}X]_{sol}[C]_{sol}$
Dead	$\frac{d[P_r]_{sol}}{dt} = \sum_j k_{tr,ij}[P_{r,i}\cdot]_{sol}[M_j]_{sol} + \sum_i\sum_j\sum_{s=0}^{r}k_{tc,ij}[P_{r,i}\cdot]_{sol}[P_{r-s,j}\cdot]_{sol}$ $+ \sum_i\sum_j\sum_{s=0}^{r}k_{td,ij}[P_{r,i}\cdot]_{sol}[P_{s,j}\cdot]_{sol}$

TABLE 3 Definition of Pseudo-Kinetic Rate Constants

Type of Reaction	Definition of Pseudo-Kinetic Rate Constants[a]
Propagation	$\overline{k_p}=\sum_{i=1}^{N}\sum_{j=1}^{N}k_{p,ij}\phi_i f_i$
ATRP Equilibrium	$\overline{k_a}=\sum_{i=1}^{N}k_{a,i}\tau_i$
	$\overline{k_{da}}=\sum_{i=1}^{N}k_{da,i}\phi_i$
Transfer	$\overline{k_{tr}}=\sum_{i=1}^{N}\sum_{j=1}^{N}k_{tr,ij}\phi_i f_i$
Termination	$\overline{k_{td}}=\sum_{i=1}^{N}\sum_{j=1}^{N}k_{td,ij}\phi_i\phi_j$
	$\overline{k_{tc}}=\sum_{i=1}^{N}\sum_{j=1}^{N}k_{tc,ij}\phi_i\phi_j$

[a] The mole fraction of polymer radical terminated in monomer i (ϕ_i), monomer i in the monomer mixture (f_i) and dormant chains terminated in monomer i (τ_i), are given respectively by: $\phi_i=\frac{[R_i]}{\sum_{j=1}^{N}[R_j]}$, $f_i=\frac{[M_i]}{\sum_{j=1}^{N}[M_j]}$, $\tau_i=\frac{[D_i]}{\sum_{j=1}^{N}[D_j]}$.

The subscript notation r and s denote the chain length, whereas i and j are the chain terminal unit. Specifically, there is only one monomer for homopolymerization in batch reactor ($i=j=1$), while two monomers for copolymerization in semi-batch reactor ($i=j=1$ or 2).

The molar balance equations involving solution, surface homopolymerization, and solution copolymerization are summarized and listed in Table 2, respectively. It is worth to note that as for surface homo-polymerization, the concentrations of species ($[M]_{\mathrm{sol}}$,$[C]_{\mathrm{sol}}$ and $[XC]_{\mathrm{sol}}$) in solution are in $\mathrm{mol\,L^{-1}}$, while the concentrations of species ($[P\cdot]_{\mathrm{surf}}$,$[P]_{\mathrm{surf}}$,$[PX]_{\mathrm{surf}}$ and $[RX]_{\mathrm{surf}}$) on surface are in $\mathrm{mol\,dm^{-2}}$. Therefore, we define a new parameter $\varepsilon(=S/V)$ in $\mathrm{dm^{-1}}$ for unifying the units used in mass balances equations. Accordingly, the rate constants k_{a}, k_{da}, k_{p}, and k_{tr} have the conventional unit of $\mathrm{L\,mol^{-1}s^{-1}}$, while, $k_{\mathrm{t}}^{\mathrm{surf}}$ is in $\mathrm{dm^{2}mol^{-1}s^{-1}}$.

TABLE 4 Semibatch Reactor Model

Description	Equation
Evolution of Reaction Volume (V)[a]	$\frac{dV}{dt}=V_f-\sum_{i=1}^{n}\overline{M_{n,i}}R_{p,i}V(\frac{1}{\rho_p}-\frac{1}{\rho_i})$
Evolution of Density in the Reactor	$\frac{d\rho}{dt}=\frac{V_f\rho_f}{V}-\frac{\rho}{V}\frac{dV}{dt}$
Mass Balance Equation for the ith Species	$\frac{dC_i}{dt}=\frac{1}{V}\left(V_f C_{if}-C_i\frac{dV}{dt}\right)+R_i$

[a] $\rho_{HFBMA}(g/cm^3)=1.36$; $\rho_{HEMA-TMS}(g/cm^3)=0.93$; $\rho_p(g/cm^3)=1.20$.

Pseudo-Kinetic Rate Constants

The mathematical treatment for simplifying the copolymerization procedure confirmed by previous works[29,32] is also used in this work. All the involved pseudo-kinetic rate constants in quasiliving ATRP are summarized in Table 3.

Semi-Batch Reactor Model

The semibatch reactor model is applied for synthesizing fluorinated gradient copolymers. The mass balance equations are summarized in Table 4.

Model Implementation

The main kinetic constants are summarized in Table 5 and the ode23s-function provided in MATLAB 2012b (8.0) is

TABLE 5 Kinetic Rate Constants for ATRP of HFBMA and HEMA-TMS Used in Simulation[a]

Parameter	Value	Ref.
k_{p11}	$3.80\times10^{6}\exp(-2754/T)$	57
k_{p22}	$8.99\times10^{6}\exp(-2634/T)$	58
k_{tc11}	$0.9k_{t1}=0.9\times7.1\times10^{9}\exp(-2249/T)$	59,60
k_{tc22}	$0.9k_{t2}=0.99\times10^{6}$	61
k_{td11}	$0.1k_{t1}=0.1\times7.1\times10^{9}\exp(-2249/T)$	59,60
k_{td22}	$0.1k_{t2}=1.1\times10^{5}$	61
k_{t12}, k_{t21}	$(k_{t11}\times k_{t22})^{1/2}$	62
k_{tc11}^{surf}	$0.9k_{t1}^{surf}=0.1\times6.0\times10^{14}$	42,60
k_{td11}^{surf} [b]	$0.1k_{t1}^{surf}=0.1\times6.0\times10^{14}$	42,60
r_1	0.42	63
r_2	0.66	63
k_{tr11}	$1.56\times10^{2}\exp(-2621/T)$	64
k_{tr22}	0.0122	Set to an arbitrary low value
k_{tr12}, k_{tr21}	$(k_{tr11}\times k_{tr22})^{1/2}$	Use the same method as k_t

[a] HEMA-TMS(use parameters of HEMA by analogy)

[b] Used in surface homo-polymerization system

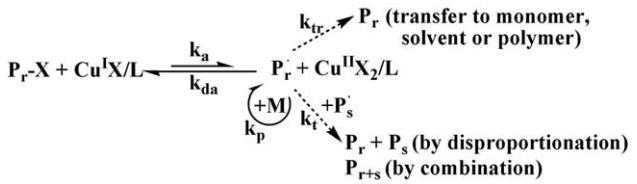

SCHEME 1 Proposed ATRP mechanism.

used to solve model equations. On the basis of definition of moments and moment equations, the polydispersity index (PDI), chain-end functionality (F_t), cumulative (F_{cum}), and instantaneous (F_{inst}) copolymer composition, etc. can be simulated from the developed model. (See the Supporting Information for details).

The least-square error calculation method used for estimating the activation and deactivation kinetic parameters is based on the set of kinetic equations as summarized in Supporting Information and two sets of experimental data (batch process) obtained in this work. In addition, due to the independence of reaction kinetic parameters on the operation mode, activation and deactivation kinetic parameters of copolymerization system in semi-batch reactor are obtained from the batch copolymerization experiments. The well estimated kinetic parameters are confirmed by the comparison of fitting data and the experimental data, and will be discussed later. All the corresponding correlation coefficients (R^2) during estimation are close to 1 (>0.98).

RESULTS AND DISCUSSION

Estimation of the Activation and Deactivation Kinetic Constants

The controlling nature of quasiliving ATRP is governed by the equilibrium between dormant and propagating radical chains as shown in Scheme 1.[65] In the activation step, the growth of chain is started through the abstraction of halogen (X) from organic initiator (RX) to transition metal/ligand catalyst in the lower oxidation state (here is Cu^IX/L). And in turn, growth chain is deactivated by the reduction of the halide complex in the higher oxidation state ($Cu^{II}X_2/L$). Accordingly, the equilibrium constant $K_{ATRP}(=k_a/k_{da})$ is crucial for designing a successful ATRP, which guarantees a controlled process.[66] In this work, according to the developed model, the estimated activation and deactivation kinetic data of micromolecular, macromolecular, and immobilized initiators using least-square method are summarized in Table 6.

For the micromolecular initiator (Eib-Br) with CuCl catalyst and 1,1,4,7,7-pentamethyldiethylenetriamine (PMDETA) ligand, the simulation result fits well with the experimental data obtained from the solution homo-polymerization of 2,2,3,3,4,4,4-heptafluorobutyl methacrylate (HFBMA) [see Fig. 1(A,B)]. The linearity of kinetic plot indicates the constant number of active species in this system. What is more, the values of k_a and k_{da} estimated in this work and extrapolated ($k_a = 1.4$ L mol^{-1}s^{-1}, $k_{da} = 1.9 \times 10^7$ L mol^{-1}s^{-1}) using the constant selectivity principle by Matyjaszewski and coworkers[50] are in the same order of magnitude, which proves the well-built model based on method of moments. The difference between the values of model estimated and the open reports is due to different experimental conditions, such as solvent, monomer, and temperature.[67]

From Figure 2(A,B), the fitting data meet quite well with experimental data obtained from CuCl/PMDETA system using macromolecular initiator (bromo-polystyrene, PS-Br, Mn = 4100 g/mol). The first-order kinetic plot for the preparing PS-b-PHFBMA diblock copolymer is linear, which indicates efficient initiation and low termination. From Table 6, the estimation value is smaller than the previously reported result ($k_a = 0.45$ L mol^{-1}s^{-1}), which was obtained directly using the GPC curve-resolution method.[68] However, it is reasonable for the relatively lower experimental temperature (80 °C) in our work than that (110 °C) of their work according to the Arrhenius formula.

Different from the solution polymerization, the radical termination involved in SI polymerization is occurring between the surface grafted propagating chains. The surface radical termination rate constant (k_t^{surf}) is found to be proportional to the catalyst concentration in solution ($k_t^{surf} \propto [C]_{sol}$) and grafting density ($\tau$) dependent following $k_t^{surf} \sim \exp(-6.4\tau)$proposed in Zhu et al.' s work.[41,42] To the best of knowledge, it is the first time to estimate the ATRP kinetics data of the immobilized spherical nanoparticles (bromo-aminopropyl functionalized SiO_2, SiO_2-APTS-Br). The simulation result in Figure 3(A,B) also fits well to the experimental data, which makes the estimated results trustworthy. The approximate linearity of the kinetic plot for surface homo-polymerization is

TABLE 6 ATRP Equilibrium Constants (K_{ATRP}) for Various Initiators with Different Ligands in Toluene at 80 °C[a]

No.	Initiator	Ligand	k_a (L mol^{-1}s^{-1})	k_{da} (L mol^{-1}s^{-1})	K_{ATRP}
1	Eib-Br[b]	PMDETA	1.43	4.5×10^7	3.2×10^{-8}
2	PS-Br[b]	PMDETA	0.35	2.2×10^7	1.6×10^{-8}
3	SiO_2-APTS-Br[b]	PMDETA	0.26	2.2×10^6	1.2×10^{-7}
4	Eib-Br[b]	dNbpy	0.25	2.1×10^7	1.2×10^{-8}
5	Eib-Br[c]	dNbpy	0.58	3.2×10^7	1.8×10^{-8}

[a] Experiments No. 1,2,4,5 were carried out using CuCl catalyst, No. 3 using $CuCl/CuCl_2$ catalyst.
[b] ATRP of HFBMA.
[c] ATRP of HEMA-TMS.

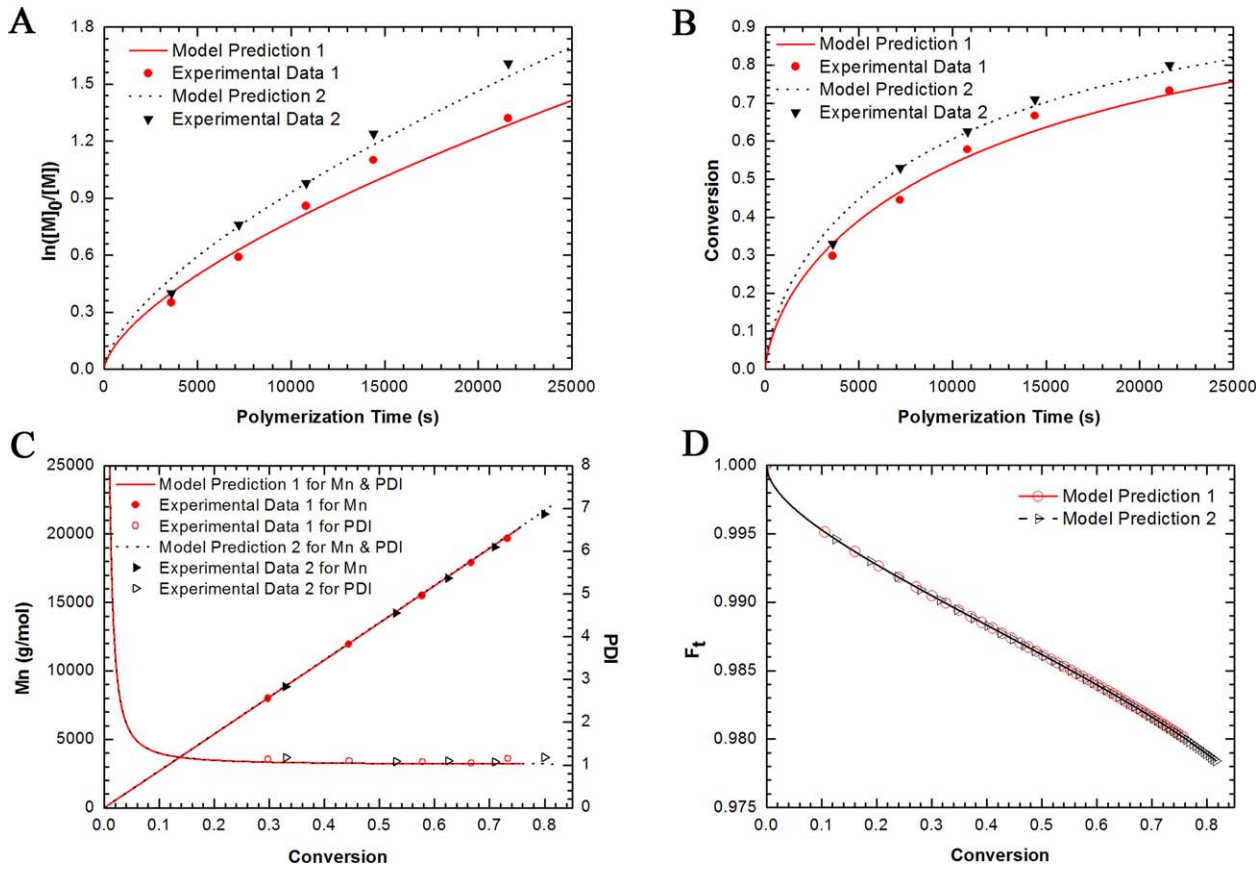

FIGURE 1 Comparison between model predictions and experimental data for batch solution ATRP of HFBMA: monomer logarithmic concentration (A) and monomer conversion (B) versus polymerization time, molecule weight/PDI (C) and end functionality (D) versus monomer conversion. Experimental condition: [HFBMA]/[CuCl]/[PMDETA]/[Eib-Br] = 100/1/2/1, $[\text{Eib-Br}]_1 = 2.40 \times 10^{-2}$mol/L for exp. 1, $[\text{Eib-Br}]_2 = 3.17 \times 10^{-2}$mol/L for exp. 2. [Color figure can be viewed in the online issue, which is available at wileyonlinelibrary.com.]

observed with the reaction proceeding, which features the quasiliving characteristic of ATRP.

The model predictions about Mn and PDI for micromolecular and macromolecular initiation systems are illustrated in Figures 1(C) and 2(C), respectively. The evolution of Mn is linear with conversion indicating quasiliving polymerization. PDI is high at low conversion and keeps leveling off after short time (<1.1), which suggests the reaction proceeds in controlled manner.

Effect of Initiator Type on ATRP Equilibrium Constant

The rate of ATRP depends strongly on the value of K_{ATRP} ($\sim 10^{-9}$ to $\sim 10^{-4}$). A high value of deactivation rate constant k_{da} ($\sim 10^{6}$ to $\sim 10^{8}$) will provide good control and produce polymers with low polydispersity.[49,50,53,56–68] However, direct measurements of K_{ATRP} and k_{da} are still difficult. In this work, we have determined the values of k_a and k_{da} for different initiators with CuCl catalyst and PMDETA ligand at 80 °C in toluene through model estimation. Thus, the K_{ATRP} values can be calculated directly from the ratio of k_a/k_{da}. As shown in Table 6, values of k_a and k_{da} decrease as the order of micromolecular, macromolecular, and immobilized initiators. By comparison, the value of k_a for Eib-Br is about four times larger than PS-Br indicating the faster activating reaction, likely due to the combination of electronic and steric effect. For electronic effect (microscopic view), ethyl isobutyrate radical is more stable than polystyrene radical due to their different electron withdrawing effects or R-X bond dissociation energies (BDEs) for the alkyl halides; for steric effect (macroscopic view), the activity of PS-Br is considered being hampered by the long carbon alkyl main chain and phenyl side chain, which influences the ability of initiation.[50,69] However, the values of k_{da} and K_{ATRP} for Eib-Br and PS-Br are large enough to keep the polymerization under control and keep consistent with opened data as proposed above.[50]

From Scheme 1, when the quasiliving ATRP equilibrium is established, the irreversible termination is only minimized rather than entirely suppressed, that is why "reversible-deactivation radical polymerization" recommended by IUPAC for this kind of polymerization.[3] Therefore, the percentage of "living" chains is below 100% (end functionality). Besides, the inevitable thermal initiation or transfer reactions (included in

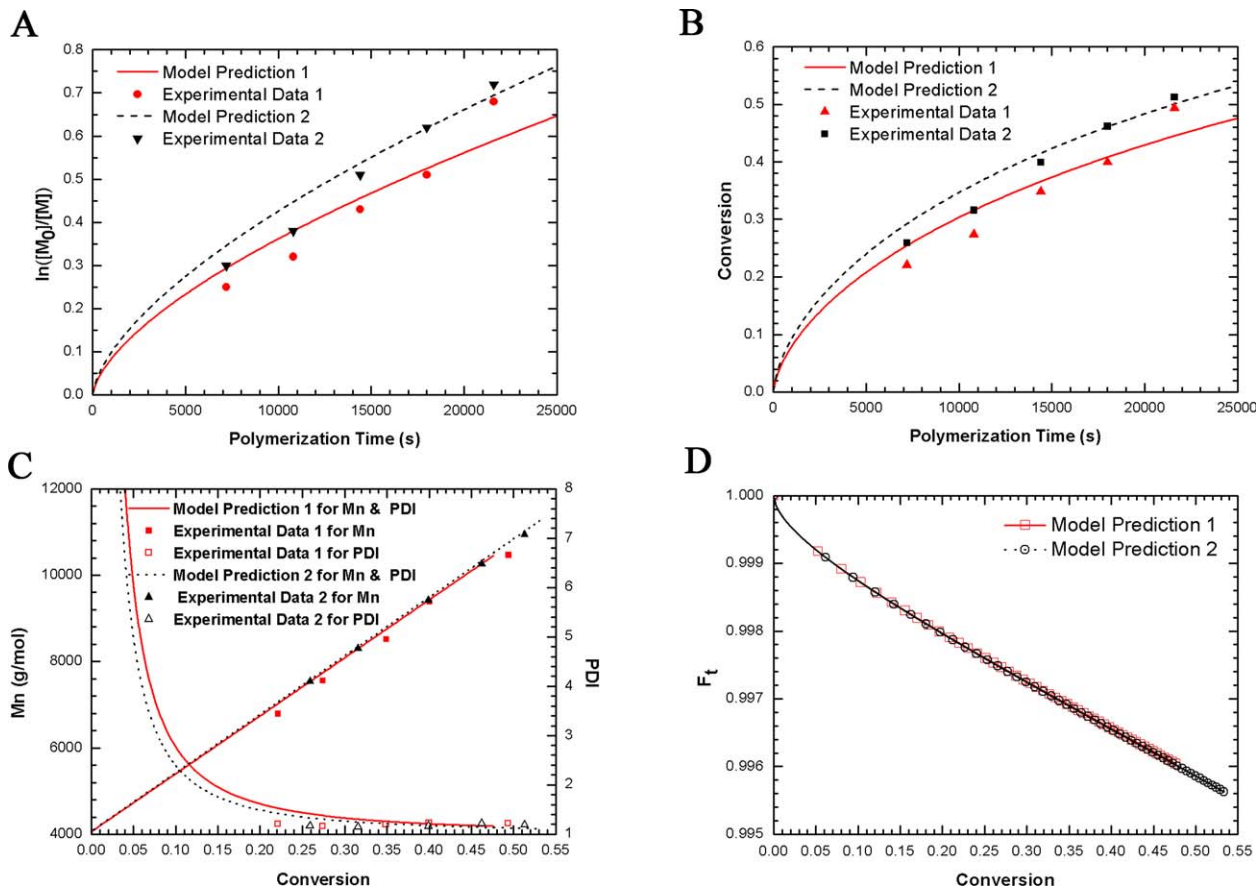

FIGURE 2 Comparison between model predictions and experimental data for batch solution ATRP of HFBMA: monomer logarithmic concentration (A) and monomer conversion (B) versus polymerization time, molecule weight/PDI (C) and end functionality (D) versus monomer conversion. Experimental condition: [HFBMA]/[CuCl]/[PMDETA]/[PS-Br] = 50/1/2/1, $[PS\text{-}Br]_1 = 3.70 \times 10^{-2}$ mol/L for exp. 1, $[PS\text{-}Br]_2 = 4.80 \times 10^{-2}$ mol/L for exp. 2. [Color figure can be viewed in the online issue, which is available at wileyonlinelibrary.com.]

model) makes the end functionality <100%. In practice, the end-group fidelity of chains is of importance for synthesizing block copolymers, but it is difficult to quantify by experiments especially in the system with high degree of polymerization. Our model predictions for chain-end functionality for micromolecular and macromolecular initiation systems are illustrated in Figures 1(D) and 2(D), respectively.

In all simulations, the "livingness" of polymers is extremely high at the early stages of the polymerization, and then the percentage of end-group fidelity slowly declines with conversion. With the reaction proceeding, the polymerization slows down due to the decrease of monomer concentration, as well as the termination and transfer processes competing with propagation. But, the chain-end functionality (F_t) is >0.995 for PS-Br and >0.975 for Eib-Br initiation system at the end of reaction, still implying well "living" or quasiliving feature. In the sake of preserving a high level of end functionality, stopping the polymerization at a proper monomer conversion is therefore necessary. In addition, the higher end functionality for PS-Br might be benefit from its relatively lower value of k_a as discussed above.

As for immobilized initiator polymerization system, values of k_a, k_{da}, and K_{ATRP} were first estimated and compared with those two initiators. Different from solution homopolymerization, the generated deactivator in the SI "living" polymerization is extremely low resulting from the very small amount of immobilized initiator. Therefore, extra deactivator ($CuCl_2$) is added into the studied system to ensure the sufficient deactivator in solution, which permits the control of the molecular weight.

From Table 6, one can find that the value of k_a for SiO_2-APTS-Br is even lower than that of PS-Br initiation system, which indicates the steric hindrance effect of initiator is more significant. However, even when the extra deactivator is added, the order of magnitude of k_{da} for SiO_2-APTS-Br is only to 10^6, which is one order of magnitude lower than Eib-Br and PS-Br initiation systems, and thereby makes the value of K_{ATRP} reach 1.18×10^{-7}. Although the "ideal" ATRP system should have a large value of K_{ATRP} to reduce the amount of catalyst, such a low deactivating ability might lead to the decrease of quasiliving and controllable features, which is experimentally and theoretically confirmed in

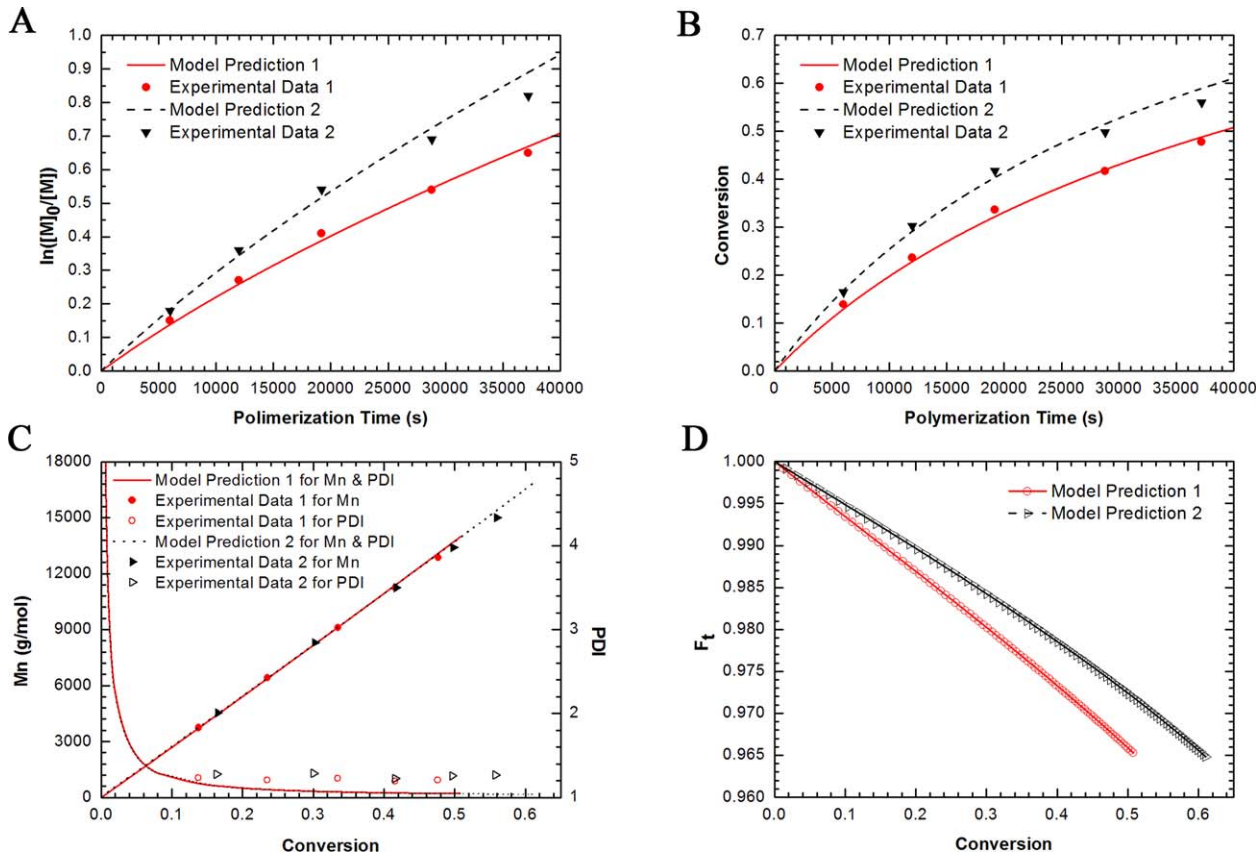

FIGURE 3 Comparison between model predictions and experimental data for batch surface-initiated ATRP of HFBMA: monomer logarithmic concentration (A) and monomer conversion (B) versus polymerization time, molecule weight/PDI (C) and end functionality (D) versus monomer conversion. Experimental condition: [HFBMA]/[CuCl]/[$CuCl_2$]/[PMDETA]/[SiO_2-APTS-Br] = 50/1/0.1/2/1, $[HFBMA]_1 = 1.375$ mol/L, for exp. 1, $[HFBMA]_2 = 1.833$ mol/L for exp. 2. [Color figure can be viewed in the online issue, which is available at wileyonlinelibrary.com.]

Figure 3(C) ($1.5 > PDI > 1.2$) and Figure 3(D) ($F_t = 0.965$). However, the extremely high radical termination ($k_t = 6.0 \times 10^{14} dm^2 mol^{-1} s^{-1}$) occurring between the chains grafted from the surface is another "culprit." It is important that the Mn plot with excellent linearity and the PDI data below 1.5 prove that the surface polymerization of HFBMA is still under quasiliving feature.

Based on the above results and analysis, the activation and deactivation kinetic constants for ATRP in different initiation systems were illustrated schematically in Scheme 2. It should be note that the limited solubility of the catalyst system (CuCl/ PMDETA complex at 80 °C in toluene) is indeed not taken into account in our kinetic modeling. However, it is reasonable for draw the conclusion based on considering the effect of a single variable (initiator type) on ATRP equilibrium constant. The kinetic constant (k_a or k_{da}) is apparent reaction rate constant, which includes an adjusting parameter describing solubility of catalyst complex.

Model Application for Preparation of Fluorinated Gradient Copolymers

The developed model coupled with semi-batch reactor model has been implemented firstly in an extended application for producing fluorinated gradient copolymer. The values of k_a and k_{da} estimated here for the copolymerization of HFBMA and 2-(trimethylsilyl)ethyl methacrylate (HEMA-TMS) using microinitiator (Eib-Br) with dNbpy ligand is smaller than those in the Eib-Br/PMDETA system listed in Table 6. It is worth noting that the bpy ligands with long alkyl groups (dNbpy) used here is due to its more soluble in less polar solvents,[69] and thus suitable for semibatch operation. Although the current catalytic system is homogeneous, the relatively lower activating ability of Eib-Br/dNbpy was illustrated in Matyjaszewski's work ($k_a = 0.60$ L $mol^{-1} s^{-1}$, $k_{da} = 2.0 \times 10^7$ L $mol^{-1} s^{-1}$, $K_{ATRP} = 3.0 \times 10^{-8}$), where concluded that activity of N-based ligands decreases with the number of coordinating sites (N4 > N3 > N2 >> N1) in ATRP.[50,69]

As for the semibatch operation, the monomer feeding rate and the choice of added monomer are two important parameters, which affect the kinetics and gradient chain structure.[29,30] Based on the developed model and known kinetic constants, the simulated results shown in Figure 4 illustrate the feeding rate affects gradient composition obviously. With feeding rate increase, the degree of polymerization decrease, but the gradient composition of resulting copolymer

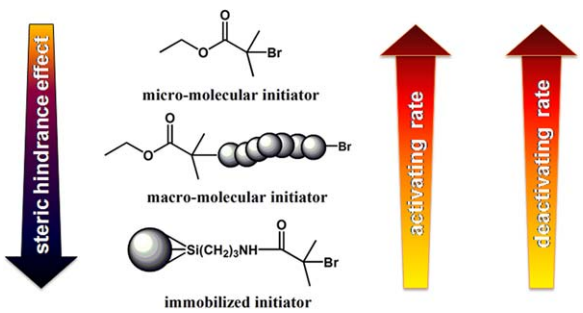

SCHEME 2 Schematic illustration of activation and deactivation kinetic constants for ATRP in different initiation systems. [Color figure can be viewed in the online issue, which is available at wileyonlinelibrary.com.]

becomes more "perfect" as it can be seen in Figure 4(A). From Figure 4(B), one can know that both monomer conversions decrease as adding rate increases, which is probably resulting from the accumulation of HFBMA in the system when feeding rate exceeds consumption rate.

Furthermore, stemming from the difference of reaction ratios, there will be having the change of composition for the linear gradient copolymers with different directions: normal linear (HFBMA in reactive flask, HEMA-TMS in airtight syringe) and inverse linear gradient copolymer (HEMA-TMS in reactive flask, HFBMA in airtight syringe). The simulation results given in Figure 5 illustrate that the effect of added monomer on the chain composition and the model predictions meet quite well with experimental data. It should be noted that the instantaneous composition (F_{inst}) of monomer in copolymer chains virtually shows a true gradient profile along a chain in contrast to the cumulative composition (F_{cum}). However, F_{inst} cannot be measured by experiment. In this work, F_{cum} of feeding monomer (HFBMA or HEMA-TMS) is measured by ^{1}H NMR. Subsequently, the corresponding F_{inst} can be calculated based on the equation: $F_{inst} = [Conv_{total,i} \times F_{cum,i} - Conv_{total,i-1} \times F_{cum,i-1}]/[Conv_{total,i} - Conv_{total,i-1}]$, where $Conv_{total}$ is the total conversion of both monomers (HFBMA and HEMA-TMS). The example of ^{1}H NMR spectrum for gradient is shown in Supporting Information.

In Figure 5(A), the instantaneous composition of HFBMA decreases from 1 to 0.1744 in normal mode, while HEMA-TMS is from 1 to 0.1739 in inverse mode. In addition, the linear relationships for the instantaneous composition imply that both patterns can produce ideal gradient composition based on appropriate monomer feeding rate (the optimal feeding rate is 1.98×10^{-7} L/s). The controllability of semi-batch ATRP can be verified through the low polydispersity and the linear increase of Mn as illustrated in Figure 5(B). Furthermore, Figure 5(C,D) show that both monomer conversions are quite different at the end of reaction, 76.46% (HFBMA) and 21.16% (HEMA-TMS) in normal linear gradient copolymerization, while 37.08% (HFBMA) and 76.21% (HEMA-TMS) in inverse linear gradient copolymerization. Finally, Figure 5(E,F) demonstrate the molecular weight (M_n) evolutions with polymer mass for normal and inverse operations are up to 15,500 and 15,850 g/mol, respectively. However, the M_n measured by GPC deviated from theoretical value at relatively higher conversion, which might be due to the poor solubility of fluorinated copolymer in THF eluent and different behavior of the copolymer in comparison with PMMA standard. As a whole, both modes can be chose for designing and producing gradient copolymer based on model by adjusting monomer feeding rate.

CONCLUSIONS

A comprehensive mathematical model was developed to investigate the effect of Eib-Br, PS-Br, and SiO_2-APTS-Br initiators on the kinetics of quasiliving ATRP of fluorinated monomer (HFBMA). The experimental and simulation results show that estimated values of k_a and k_{da} were influenced by different initiators in heterogeneous system (the highest for Eib-Br, second highest for PS-Br, and the lowest for SiO_2-APTS-Br) due to the combination of electronic and steric hindrance effects. In particular, the extremely high surface radical termination

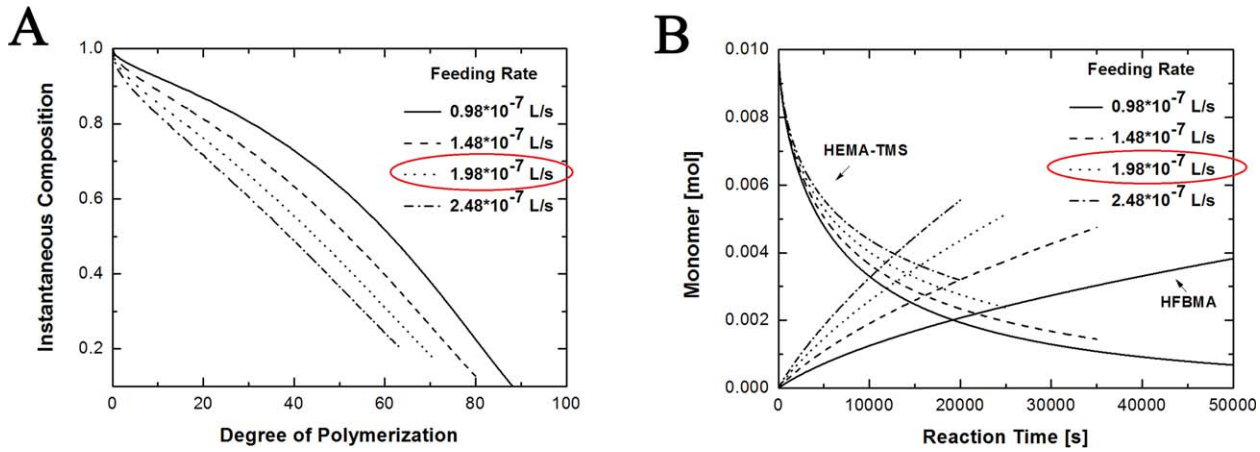

FIGURE 4 Optimal results of monomer feeding rate: instantaneous composition with degree of polymerization (A) and monomer concentration with reaction time (B). [Color figure can be viewed in the online issue, which is available at wileyonlinelibrary.com.]

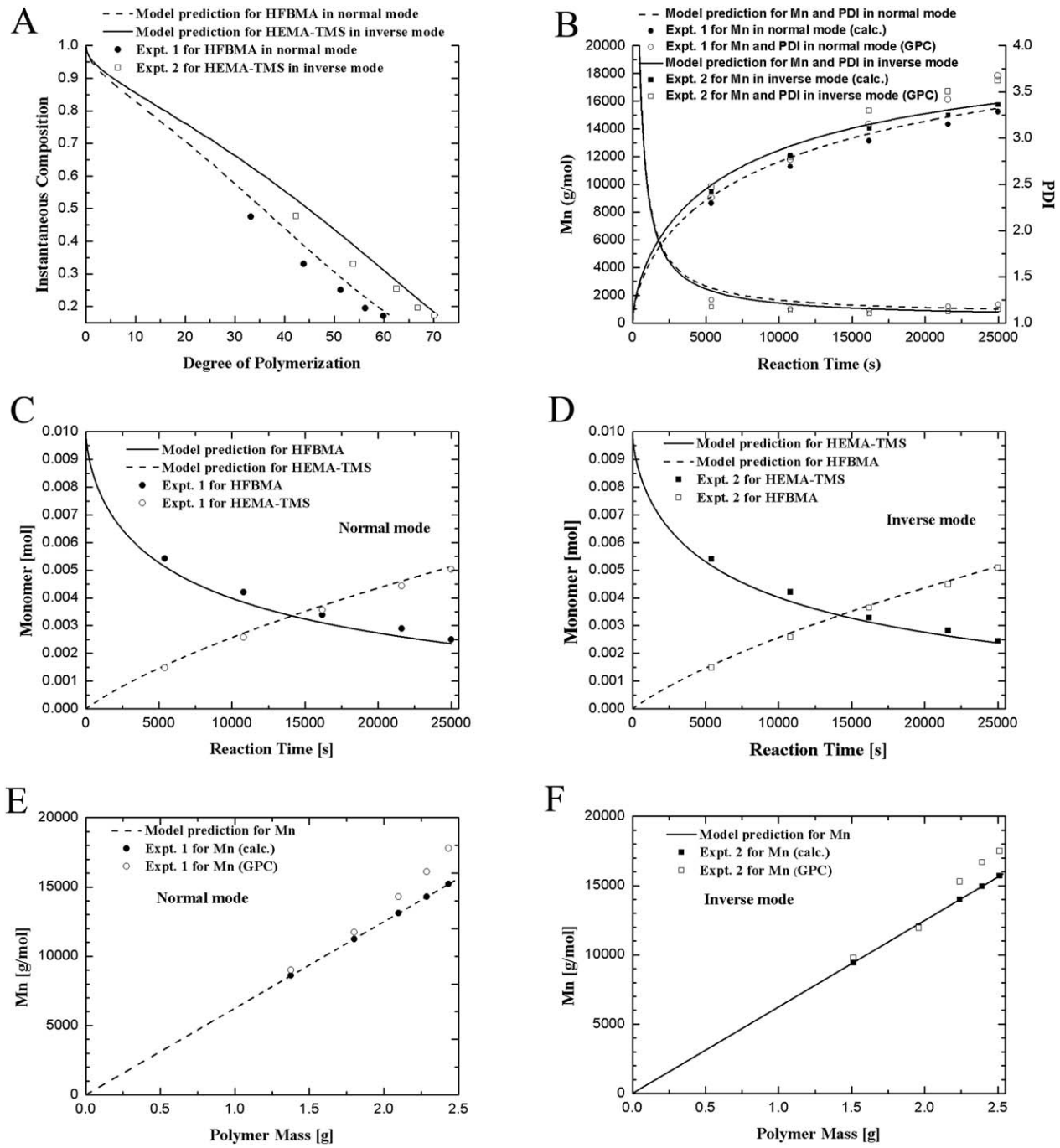

FIGURE 5 Comparison between model predictions and experimental data for producing linear (normal) and inverse linear (inverse) gradient copolymers: instantaneous composition with degree of polymerization (A), molecular weight and PDI with reaction time (B), monomer concentration with reaction time (C and D), molecular weight with polymer mass (E and F). Experimental condition: [HFBMA]/[HEMA-TMS]/[CuCl]/[dNbpy]/[Eib-Br] = 50/50/1/2/1, Normal mode: [Eib-Br] = 3.98×10^{-2} mol/L, $V_f = 2.02 \times 10^{-7}$ L/s; Inverse mode: [Eib-Br] = 3.90×10^{-2} mol/L, $V_f = 1.98 \times 10^{-7}$ L/s.

($k_t = 6.0 \times 10^{14} \mathrm{dm}^2 \mathrm{mol}^{-1} \mathrm{s}^{-1}$) for the SiO_2-APTS-Br initiation system results in the decrease of k_{da}, and thus increases the value of K_{ATRP} even when extra deactivator is added, which gives rise to less quasiliving feature than solution ATRP.

When extending the model to Eib-Br with Cu^ICl/dNbpy homogeneous catalytic complexes initiation system, the relatively lower activating ability (the value is ~3 times smaller than that of PDMETA) is found ascribing to its less coordinating sites than Cu^ICl/PMDETA initiation system, which was also illustrated in Matyjaszewski's work (the value is ~5 times smaller than that of PDMETA).[50,69] But the polymerization keeps controllable by its higher deactivating ability. After that, the kinetic model coupling with semi-batch

reactor model was used to optimize feeding rate and study the influence of monomer added on the gradient composition of fluorinated copolymer.

In summary, this work is useful for further understanding the structure-activity relationship for the ligand and initiators in quasiliving ATRP. With the well estimated equilibrium constants by the developed model, it is possible to design and predict the copolymer chain composition in semi-batch reactor.

ACKNOWLEDGMENTS

The authors thank the National Natural Science Foundation of China (No. 21276213), the National 863 plan project of China (No. 2013AA032302), the Research Fund for the Doctoral Program of Higher Education (No. 20130073110077) and the Key Laboratory of Advanced Control and Optimization for Chemical Processes of the National Ministry of Education of China (No. 2012ACOCP03) for supporting this work.

NOMENCLATURE

C	Activator and catalyst at the lower oxidation state
CX	Deactivator and catalyst at the higher oxidation state
C_i	Concentration of the species i in the reactor (mol m^{-3})
$C_{i,f}$	Concentration of the species i in the feed, (mol m^{-3})
$k_{a,i}$	Activation rate constant for dormant chain with i-type of terminal unit (L mol^{-1} s^{-1})
$k_{da,i}$	Deactivation rate constant for radical with i-type of terminal unit, (L mol^{-1} s^{-1})
$k_{p,ij}$	Chain propagation rate constant for monomer j adding to radical with i-type of terminal unit, (L mol^{-1} s^{-1})
$k_{tr,ij}$	Chain transfer rate constant for monomer j adding to radical with i-type of terminal unit, (L mol^{-1} s^{-1})
$k_{tc,ij}$	Combinative termination rate constant between radicals with i and j types of terminal unit, (L mol^{-1} s^{-1}) or (dm^2 mol^{-1} s^{-1})
$k_{td,ij}$	Disproportional termination rate constant between radicals with i and j types of terminal unit, (L mol^{-1} s^{-1}) or (dm^2 mol^{-1} s^{-1})
$\overline{M_{n,i}}$	Number molecular weight of monomer i, (g mol^{-1})
M_i	Monomer i
$P_0\cdot$	Primary radical
P_0X	Initiator
P_r	Dead chain with length r
P_s	Dead chain with length s
$P_{r,i}\cdot$	Propagating radical chain with length r and i-type of terminal unit
$P_{r,i}X$	Dormant chain with length r and i-type of terminal unit
r_i	Reactivity ratio of monomer i
$R_{p,i}$	Intrinsic propagation rate of the monomer i (mol m^{-3} s^{-1})
R_i	Intrinsic reaction rate of the species i (mol m^{-1} s^{-1})
R	Gas constant (J K^{-1} mol^{-1})
T	Temperature (K)
V_i	Volume of species i (m^3)
V	Volume of total system (m^3)
V_f	Volumetric feeding rate, (m^3 s^{-1})
τ^m	mth-order moment of dead chain
λ_i^m	mth-order moment of dormant chain with i-type of terminal unit
μ_i^m	mth-order moment of propagating radical with i-type of terminal unit
v_f	Free volume fraction (cm^3 s^{-1})
v_{f0}	Free volume fraction (cm^3 s^{-1})
ρ	Density of reaction mixture (g cm^{-3})
ρ_i	Density of component i (g cm^{-3})
ρ_f	Density of feeding materials (g cm^{-3})
0	Value at initial conditions
1	HFBMA
2	HEMA-TMS
M	Monomer
P	Polymer
S	Solvent

REFERENCES AND NOTES

1 B. Iván, *Macromol. Chem. Phys.* **2000**, *201*, 2621–2628.

2 K. Verebélyi, Á. Szabó, B. Iván, *Polymer* **2012**, *53*, 4940–4946.

3 A. D. Jenkins, R. G. Jones, G. Moad, *Pure Appl. Chem.* **2010**, *82*, 483–491.

4 W. A. Braunecker, K. Matyjaszewski, *Prog. Polym. Sci.* **2007**, *32*, 93–146.

5 M. Ouchi, T. Terashima, M. Sawamoto, *Chem. Rev.* **2009**, *109*, 4963–5050.

6 B. Ameduri, *Macromolecules* **2010**, *43*, 10163–10184.

7 B. Ameduri, *Chem. Rev.* **2009**, *109*, 6632–6686.

8 F. Boschet, B. Ameduri, *Chem. Rev.* **2014**, *114*, 927–980.

9 Z. H. Luo, T. Y. He, *React. Funct. Polym.* **2008**, *68*, 931–942.

10 H. Cheng, J. J. Li, Z. H. Luo, *J. Polym. Sci. Part A: Polym. Chem.* **2012**, *50*, 1249–1253.

11 Y. Z. Zhou, H. Cheng, Z. H. Luo, *J. Polym. Sci. Part A: Polym. Chem.* **2011**, *49*, 3647–3657.

12 J. J. Wang, Y. N. Zhou, P. Wang, Z. H. Luo, *RSC Adv.* **2013**, *3*, 5045–5055.

13 J. Chen, J. J. Li, Z. H. Luo, *J. Polym. Sci. Part A: Polym. Chem.* **2013**, *51*, 1107–1117.

14 T. Von Werne, T. E. Patten, *J. Am. Chem. Soc.* **2001**, *123*, 7497–7505.

15 J. Pyun, S. Jia, T. Kowalewski, G. D. Patterson, K. Matyjaszewski, *Macromolecules* **2003**, *36*, 5094–5104.

16 K. Ohno, T. Morinaga, K. Koh, Y. Tsujii, T. Fukuda, *Macromolecules* **2005**, *38*, 2137–2142.

17 R. E. Behling, B. A. Williams, B. L. Staade, L. M. Wolf, E. W. Cochran, *Macromolecules* **2009**, *42*, 1867–1872.

18 H. J. Yu, Z. H. Luo, *J. Polym. Sci. Part A: Polym. Chem.* **2010**, *48*, 5570–5580.

19 H. J. Yu, Z. H. Luo, *J. Polym. Sci. Part A: Polym. Chem.* **2011**, *49*, 174–183.

20 H. J. Yu, Z. H. Luo, *Polym. Eng. Sci.* **2011**, *51*, 218–224.

21 S. P. Zhu, *Macromol. Theory Simul.* **1999**, *8*, 29–37.

22 O. Delgadillo-Velazquez, E. Vivaldo-Lima, I. A. Quintero-Ortega, S. P. Zhu, *AIChE J.* **2002**, *18*, 2597–2608.

23 X. Li, W. J. Wang, B. G. Li, S. P. Zhu, *Macromol. React. Eng.* **2011**, *5*, 467–478.

24 R. Wang, Y. W. Luo, B. G. Li, S. P. Zhu, *AIChE J.* **2007**, *53*, 174–186.

25 Y. Zhao, Y. W. Luo, C. H. Ye, B. G. Li, S. P. Zhu, *J. Polym. Sci. Part A: Polym. Chem.* **2009**, *47*, 69–79.

26 H. Tobita, *Macromol. Theory Simul.* **2007**, *16*, 810–823.

27 H. Tobita, *Macromol. React. Eng.* **2010**, *4*, 643–662.

28 H. Tobita, *Macromol. Theory Simul.* **2011**, *20*, 179–190.

29 Y. N. Zhou, J. J. Li, Z. H. Luo, *J. Polym. Sci. Part A: Polym. Chem.* **2012**, *50*, 3052–3066.

30 Y. N. Zhou, Z. H. Luo, J. H. Chen, *AIChE J.* **2013**, *59*, 3019–3033.

31 Y. Huang, Y. N. Zhou, Q. Zhang, Z. H. Luo, *J. Appl. Polym. Sci.* **2013**, *130*, 3473–3481.

32 M. Al-Harthi, J. B. P. Soares, L. C. Simon, *Macromol. React. Eng.* **2007**, *1*, 468–479.

33 M. Al-Harthi, J. K. Masihullah, S. H. Abbasi, J. B. P. Soares, *Macromol. Theory Simul.* **2009**, *18*, 307–316.

34 M. Al-Harthi, M. J. Khan, S. H. Abbasi, J. B. P. Soares, *Macromol. React. Eng.* **2009**, *3*, 148–159.

35 D. R. D'Hooge, M. F. Reyniers, G. B. Marin, *Macromol. React. Eng.* **2009**, *3*, 185–209.

36 D. R. D'Hooge, M. F. Reyniers, F. J. Stadler, B. Dervaux, C. Bailly, F. E. Du Prez, G. B. Marin, *Macromolecules* **2010**, *43*, 8766–8781.

37 D. R. D'Hooge, D. Konkolewicz, M. F. Reyniers, G. B. Marin, K. Matyjaszewski, *Macromol. Theory Simul.* **2012**, *21*, 52–69.

38 K. A. Payne, D. R. D'Hooge, P. H. M. Van Steenberge, M. F. Reyniers, M. F. Cunningham, R. A. Hutchinson, G. B. Marin, *Macromolecules* **2013**, *46*, 3828–3840.

39 D. Xiao, M. J. Wirh, *Macromolecules* **2002**, *35*, 2919–2925.

40 J. B. Kim, W. Huang, D. Miller, G. L. Baker, M. L. Bruening, *J. Polym. Sci. Part A: Polym. Chem.* **2003**, *41*, 386–394.

41 X. Gao, W. Feng, S. P. Zhu, H. Sheardown, J. L. Brash, *Macromol. React. Eng.* **2010**, *4*, 235–250.

42 D. Zhou, X. Gao, W. J. Wang, S. P. Zhu, *Macromolecules* **2012**, *45*, 1198–1207.

43 S. Turgman-Cohen, J. Genzer, *Macromolecules* **2010**, *43*, 9567–9577.

44 S. Turgman-Cohen, J. Genzer, *J. Am. Chem. Soc.* **2011**, *133*, 17567–17569.

45 B. Guyot, B. Ameduri, B. Boutevin, *J. Fluorine Chem.* **1995**, *74*, 233–240.

46 B. Guyot, B. Ameduri, B. Boutevin, A. Sideris, *Macromol. Chem. Phys.* **1995**, *196*, 1875–1886.

47 B. Guyot, B. Ameduri, B. Boutevin, M. Melas, M. Viguier, A. Collet, *Macromol. Chem. Phys.* **1998**, *199*, 1879–1885.

48 J. D. Jeyaprakash, S. Samuel, R. Dhamodharan, J. Rühe, *Macromol. Rapid Commun.* **2002**, *23*, 277–281.

49 W. Tang, N. V. Tsarevsky, K. Matyjaszewski, *J. Am. Chem. Soc.* **2006**, *128*, 1598–1604.

50 W. Tang, Y. Kwak, W. Braunecker, N. V. Tsarevsky, M. L. Coote, K. Matyjaszewski, *J. Am. Chem. Soc.* **2008**, *130*, 10702–10713.

51 F. Seeliger, K. Matyjaszewski, *Macromolecules* **2009**, *42*, 6050–6055.

52 W. A. Braunecker, N. V. Tsarevsky, A. Gennaro, K. Matyjaszewski, *Macromolecules* **2009**, *42*, 6348–6360.

53 S. Faucher, P. Okrutny, S. Zhu, *Ind. Eng. Chem. Res.* **2007** *46*, 2726–2734.

54 C. Boyer, D. Valade, P. Lacroix-Desmazes, B. Ameduri, B. Boutevin, *J. Polym. Sci. Part A: Polym. Chem.* **2006**, *44*, 5763–5777.

55 J. Morick, M. Buback, K. Matyjaszewski, *Macromol. Chem. Phys.* **2012**, *213*, 2287–2292.

56 Y. Wang, Y. Kwak, J. Buback, M. Buback, K. Matyjaszewski, *ACS Macro. Lett.* **2012**, *1*, 1367–1370.

57 S. Beuermann, M. Buback, T. P. Davis, R. G. Gilbert, R. A. Hutchinson, A. Kajiwara, B. Klumperman, G. T. Russell, *Macromol. Chem. Phys.* **2000**, *201*, 1355–1364.

58 M. Buback, C. H. Kurz, *Macromol. Chem. Phys.* **1998**, *199*, 2301–2310.

59 M. Buback, T. Junkers, *Macromol. Chem. Phys.* **2006**, *207*, 1640–1650.

60 Y. Fu, A. Mirzaei, M. F. Cunningham, R. A. Hutchinson, *Macromol. Symp.* **2007**, *259*, 151–163.

61 M. D. Goodner, H. R. Lee, C. N. Bowman, *Ind. Eng. Chem. Res.* **1997**, *36*, 1247–1252.

62 C. Walling, *J. Am. Chem. Soc.* **1949**, *71*, 1930–1935.

63 K. Liang, R. A. Hutchinson, *Macromolecules* **2010**, *43*, 6311–6320.

64 D. H. Li, M. C. Grady, R. A. Hutchinson, *Ind. Eng. Chem. Res.* **2005**, *44*, 2506–2517.

65 J. S. Wang, K. Matyjaszewski, *J. Am. Chem. Soc.* **1995**, *117*, 5614–5615.

66 M. Horn, K. Matyjaszewski, *Macromolecules* **2013**, *46*, 3350–3357.

67 A. K. Nanda, K. Matyjaszewski, *Macromolecules* **2003**, *36*, 1487–1493.

68 K. Ohno, A. Goto, T. Fukuda, J. Xia, K. Matyjaszewski, *Macromolecules* **1998**, *31*, 2699–2701.

69 W. Tang, K. Matyjaszewski, *Macromolecules* **2006**, *39*, 4953–4959.